JOURNAL OF AIRCRAFT
Vol. 41, No. 5, September–October 2004

Structure and Induced Drag of a Tip Vortex

D. Birch* and T. Lee†
McGill University, Montreal, Quebec H3A 2K6, Canada
and
F. Mokhtarian‡ and F. Kafyeke§
Bombardier Aerospace, Dorval, Quebec H4S 1Y9, Canada

The three-dimensional flow structure of a tip vortex in the near wake of both a rectangular, square-tipped NACA 0015 airfoil and a high-lift cambered airfoil was investigated by using a seven-hole pressure probe at $Re = 2.01 \times 10^5$. Lift-induced drag was computed based on vorticity and was compared with force-balance data. For both the airfoils tested, the vortex strength reached a maximum immediately behind the trailing edge and remained nearly constant up to two chord lengths downstream. As the airfoil incidence increased, the increase in the lift force resulted in a basically linear increase in the vortex strength and the peak values of the tangential velocity and vorticity, whereas the vortex radius did not appear to have a clear dependence on the vortex strength. Depending on the airfoil incidence, the core axial velocity could be wake-like or jet-like. The normalized circulation within the inner region of the nearly axisymmetric tip vortex exhibited a universal, or self-similar, structure. The NACA 0015 airfoil, however, possessed smaller tangential velocities but similar vortex core diameters compared to those of a cambered airfoil.

Nomenclature

b	=	airfoil span
C_{Di}	=	induced drag coefficient, $= D_i/\frac{1}{2}\rho u_\infty^2 bc$
C_{Dp}	=	profile drag coefficient of a three-dimensional wing configuration
$C_{D,2\text{-}d}$	=	total drag coefficient of a two-dimensional wing configuration
$C_{D,3\text{-}d}$	=	total drag coefficient of a three-dimensional wing configuration, $= C_{\mathrm{Dp}} + C_{\mathrm{Di}}$
$C_{L,2\text{-}d}$	=	lift coefficient of a two-dimensional wing configuration, $= L/\frac{1}{2}\rho u_\infty^2 bc$
$C_{L,3\text{-}d}$	=	lift coefficient of a three-dimensional wing configuration
c	=	airfoil chord
D_i	=	induced drag
D_p	=	profile drag
$D_{2\text{-}d}$	=	total drag of a two-dimensional wing configuration
$D_{3\text{-}d}$	=	total drag of a three-dimensional wing configuration, $= D_p + D_i$
L	=	lift
P	=	pressure
Re	=	chord Reynolds number, $= u_\infty c/\nu$
r	=	radial position
r_c	=	vortex core radius
r_o	=	vortex outer radius
u_a	=	axial velocity
$u_{\mathrm{a,c}}$	=	core axial velocity
u_∞	=	freestream velocity
v	=	spanwise mean velocity
v_θ	=	tangential velocity
w	=	transverse mean velocity
x	=	streamwise or axial direction
y	=	spanwise direction
z	=	transverse direction
α	=	angle of attack
α_{ss}	=	static-stall angle
Γ	=	vortex strength or circulation
Γ_c	=	core vortex strength
Γ_0	=	total vortex strength
ζ	=	streamwise vorticity, $= \partial w/\partial y - \partial v/\partial z$
ν	=	fluid kinematic viscosity
ρ	=	fluid density
σ	=	source term in equation 4, $= \partial v/\partial y + \partial w/\partial z$
ϕ	=	velocity potential
ψ	=	stream function

Received 28 May 2003; revision received 29 August 2003; accepted for publication 9 September 2003.

*Ph.D. Research Assistant, Department of Mechanical Engineering.
†Associate Professor, Department of Mechanical Engineering. Member AIAA.
‡Section Chief, Advanced Aerodynamics, Department 777. Member AIAA.
§Manager, Advanced Aerodynamics, Department 777. Senior Member AIAA.

I. Introduction

THE counter-rotating vortices generated by an aircraft wing tip, because of their hazardous effects on flight safety, continue to be of concern to aviation and aircraft manufacturers alike. The recent winglet retrofit order of Southwest Airline for 169 737-700/800, capable of saving 92,000 gallons of fuel per year per aircraft,[1] further reinforces the paramount importance of the wing-tip vortex and its control. Moreover, tip vortices shed from helicopter rotor blades and propellers interact with following blades causing rotor noise and vibration. Therefore, in order to minimize the separation time of aircraft during takeoff, as well as to reduce the tip-vortex-induced drag and noise, the tip-vortex wake characteristics must be measured and predicted accurately and reduced or eliminated, if possible, so as to allow the most efficient use of airport facilities and to ensure flight safety and efficiency.

Numerous experimental, theoretical, and computational investigations have been conducted to improve the understanding of the tip-vortex structure and its dissipation or persistence, as well as its control. However, unlike the usual void of experimental data, a substantial effort[2–13] has been invested in developing theoretical and numerical models for the roll-up process of tip vortices. The bulk of the experimental effort has been directed mainly toward finding the rate of change of the tangential velocity and the strength of trailing vortices in the mediate or far-field regions, while addressing the issues of vortex development, stability, and breakdown. However, only limited experiments[14–19] have been conducted to investigate the dynamics of the initial roll up of a tip vortex around

the wing tip and its subsequent development in the near field of an airfoil. The near-field behavior of a tip vortex is significant in both fixed- and rotary-wing aerodynamics, including the flow behind canard wings, helicopter blades (a major noise source), sails of submarines, and propeller blades (where the control of tip vortex cavitation is of extreme importance in reducing noise and wear). Devenport et al.[16] investigated the tip-vortex structure in the range of 5–30 chord lengths downstream of a NACA 0012 airfoil with a blunt tip at $Re = 5.3 \times 10^5$ by using a miniature four-sensor hot-wire probe. Chow et al.[17] investigated the tip-vortex flow (up to 0.678 chord lengths downstream of the trailing edge) of a NACA 0012 airfoil model with a rounded tip at $Re = 4.6 \times 10^6$ by using a seven-hole pressure probe and a triple hot-wire probe. However, despite much work, there is obviously still a need to improve our understanding of the initiation, growth, and development of tip vortices. An improved understanding of the near field of a tip vortex and its control will result in an aerodynamic advantage through a reduction in induced drag.

The objective of this study was to characterize the roll up and development of a tip vortex both along the tip and in the near wake (up to two chord lengths downstream of the trailing edge) of a square-tipped, rectangular NACA 0015 airfoil and also of a high-lift cambered airfoil by using a miniature seven-hole pressure probe. Special attention was given to the effects of airfoil incidence α and downstream distance on the behavior and variation of the vortex strength and size and the crossflow and axial velocity distributions of the tip vortex. The tip-vortex measurements were then used to determine the magnitudes of the induced drag and were compared to the wind-tunnel force-balance data.

II. Experimental Apparatus and Methods

The experiments were carried out in a $0.9 \times 1.2 \times 2.7$ m suction-type subsonic wind tunnel with a freestream turbulence intensity of 0.08% at 50 m/s. A square-tipped, rectangular NACA 0015 airfoil and a high-lift Bombardier R&D wing with no twist (Fig. 1a), each with a chord c of 25.4 cm and a span b of 37.9 cm, were used to generate the tip vortex. The freestream velocity u_∞ was fixed at 12.3 m/s, which rendered a chord Reynolds number Re of 2.01×10^5. The airfoil model was mounted vertically at the center of the bottom wall of the wind-tunnel test section. The origin of the coordinates was located at the leading edge of the airfoil with x, y, and z aligned with the streamwise, spanwise, and transverse directions, respectively. A miniature seven-hole pressure probe (with an outside diameter of 2.7 mm) was used to measure the three mean velocity components (u, v, and w). The probe was calibrated in situ, following the calibration procedures described by Wenger and Devenport,[20] before the installation of the model. Eight pressure transducers (seven for the probe and one for tunnel reference total) were used to maximize the data rate of the probe measurement system at each measurement location. The pressure signals were sampled at 500 Hz, with a sampling time of 10 s, and were recorded on a Pentium II PC through a 16-bit A/D converter board. Probe traversing was achieved through a custom-built computer-controlled traversing system. Mean tip-vortex flowfield measurements were made at crossflow planes located between $x/c = 0.5$–3 for $\alpha = 10$ deg, and also at $x/c = 1.5$ for $\alpha = 2 - 18$ deg. Data planes taken along the tip and in the near field of the wing models had 49×49 measuring grid points with an increment of $\Delta y = \Delta z = 3.2$ mm. Finer $\Delta y = \Delta z =$ 1.6 mm were also used in the determination of the vortex-core characteristics.

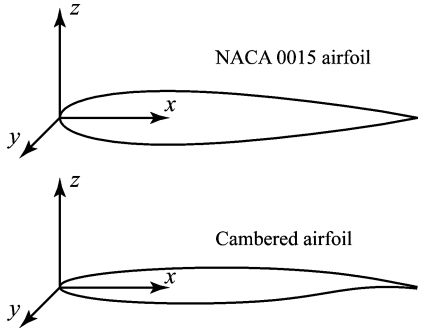

Fig. 1a Geometry and coordinate of the airfoil models.

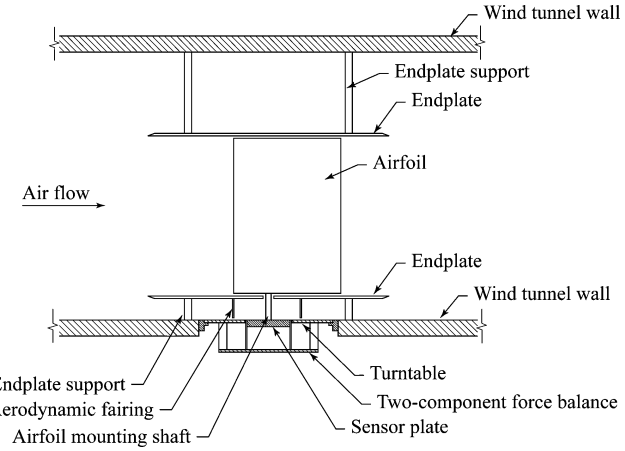

Fig. 1b Schematic of the force-balance measurement system.

For lift- and drag-force measurements, the models were mounted vertically on an external two-component force balance located below the wind tunnel (Fig. 1b). The airfoil model was mounted vertically between two $0.45 \times 60 \times 60$ cm aluminum endplates with sharp leading edges. The bottom plate was fixed to the bottom wall of the test section, and an aerodynamic fairing was placed around the shaft to isolate it from the tunnel flow. The top endplate was mounted on the top wall of the test section. The gaps between the airfoil and the endplates were kept at less than 1 mm to minimize leakage of flow through the gaps. This configuration approximated an airfoil with an effective aspect ratio of infinity and will hereafter be referred to as the two-dimensional wing configuration. Furthermore, by removing the top endplate and the supports, the total lift, $C_{L,3\text{-}d}$, and drag $C_{D,3\text{-}d}$, coefficients of a three-dimensional wing configuration were also obtained. The maximum experimental uncertainties in the results reported have been estimated as follows: mean velocity 3.5%, vorticity component 9%, and vortex radius 4%. No wind-tunnel wall corrections were made to the present measurements.

III. Results and Discussion

A. Velocity and Vorticity Distributions

Figure 2 shows the representative normalized streamwise vorticity ($\zeta c/2u_\infty$) contours of a tip vortex for $x/c = 0.5$–2.5 at $\alpha = 10$ deg for both the airfoil models tested. The presence of the multiple secondary vortices at $x/c = 0.5$ and their wrapping around the main vortex as they progressed down the chord can be clearly seen from the vorticity contours. As x/c increased, the region of high vorticity increased (in both area and magnitude) as the main vortex gained strength from the feeding sheet of boundary-layer vorticity, and these secondary structures were eventually entrained by the main tip vortex. Downstream of the trailing edge of the wing, the rapid shear layer roll-up process caused the vorticity from the shear layer leaving the trailing edge to be carried into the core region of the vortex. At $x/c \approx 1.5$, a nearly axisymmetric tip vortex with nearly uniform spacing of the vorticity contours already existed in the inner region of the vortex. The remainder of the vorticity decreased gradually from a maximum at the center to nearly zero in the outer part of the vortex. Outside the core the flow structure was dominated by the remainder of the wing wake, which wound into an ever-increasing spiral. For the cambered airfoil, however, the flow structure around the vortex core was found to be more axisymmetric and tightly wound (i.e., with less diffusion) and with much higher vorticity levels, and the presence of secondary vortices was also more evident. Composite plots of the normalized vorticity contours and axial-flow contours as functions of α and x/c are presented in Fig. 3. Figure 3 also indicates that the axial velocity within the

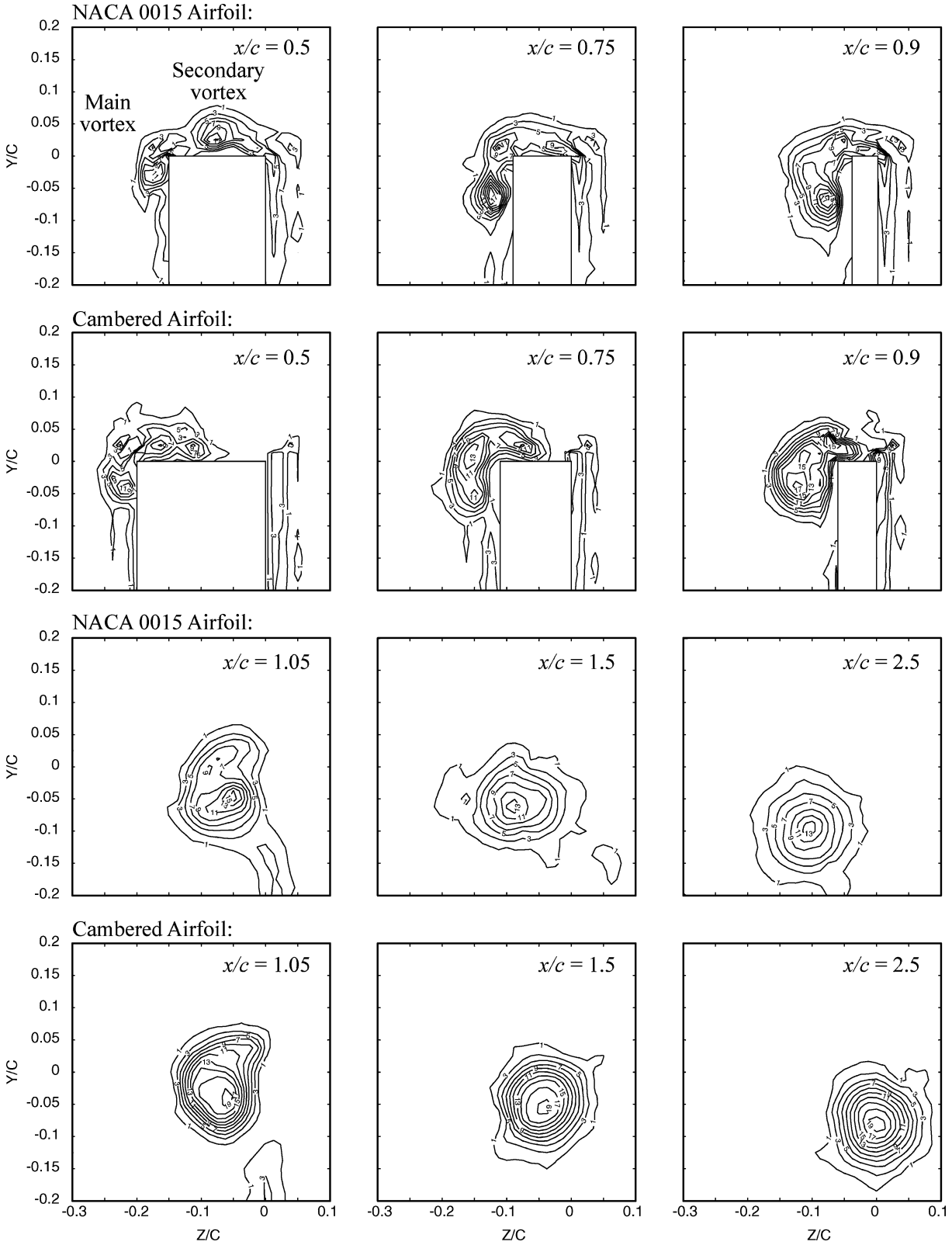

Fig. 2 Typical normalized vorticity contours for $\alpha = 10$ deg. Numerical values denote $\zeta c/2u_\infty$ levels.

viscous wake that was shed from the wing was observed to form islands of axial velocity both exceeded and fell behind the freestream value.

Figure 4 shows the typical distributions of the normalized z-component flow quantities (i.e., the tangential v_θ and axial u_a velocities and vorticity) across the vortex center for $\alpha = 4$, 8, and 12 deg at $x/c = 1.5$. As expected, v_θ changed sign from negative to positive as one crossed the vortex core from inboard to outboard, a behavior typical of a tip vortex (Fig. 4a). The core-flow region in which v_θ varied nearly linearly with the radius was identified by the constant slope of the curve. Outside the core-flow region the tangential velocity varied inversely with the radius and asymptotically approached a value of zero. The vorticity was highest at the center of the vortex and approached zero outside of the core (Fig. 4c). In Fig. 4b, the double-bell, wake-like velocity profile shows that the vortex core axial flow switched from being wake-like to jet-like at

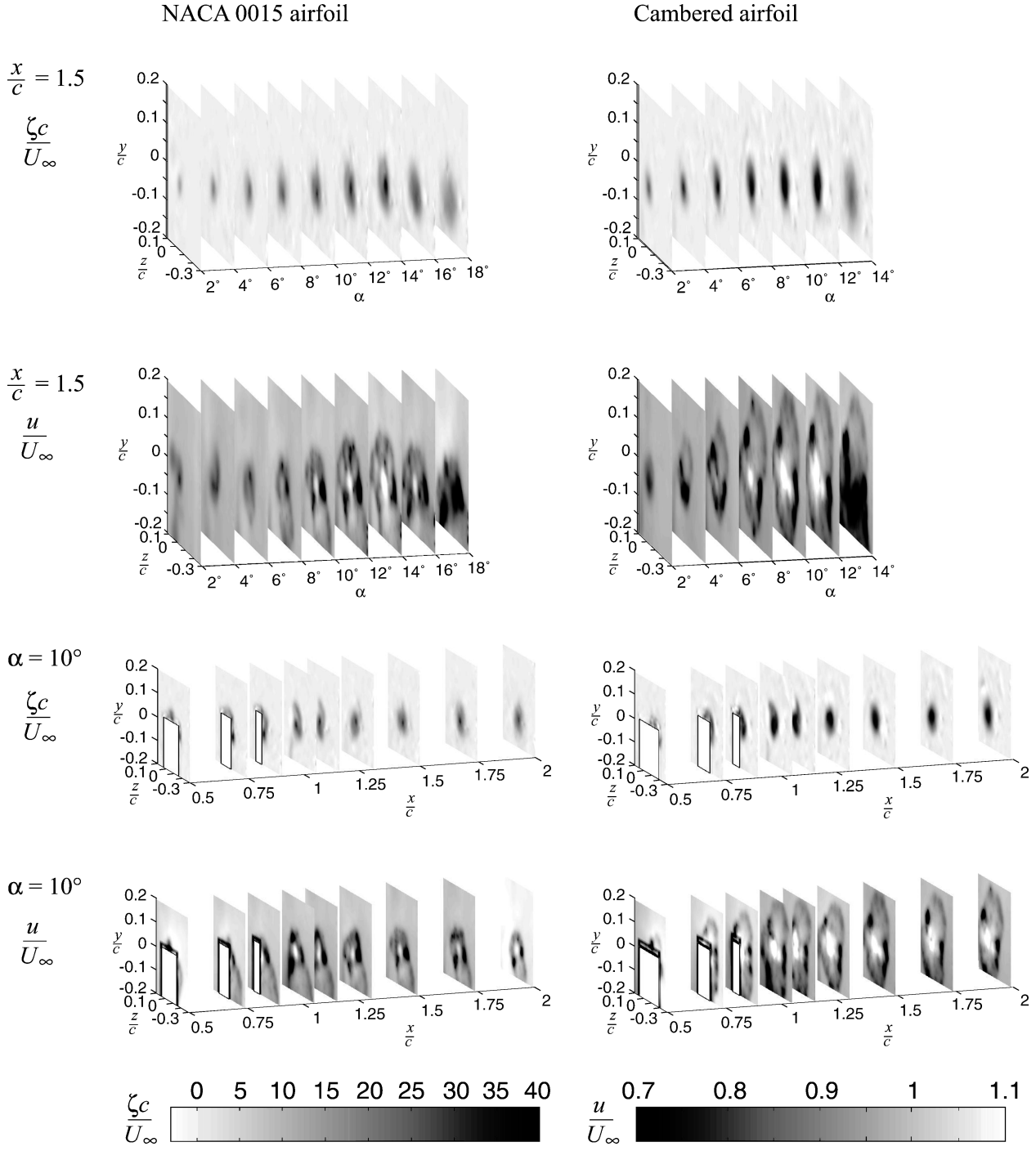

Fig. 3 Composite plots of tip-vortex flow structures at different α and x/c.

$\alpha \approx 8$ and 6 deg for the NACA 0015 and cambered airfoil models, respectively. Furthermore, for $x/c \geq 1.5$ the vortex flow quantities of both the airfoils tested resembled those of typical asymptotic trailing vortices.

B. Peak Vortex Flow Quantities and Size

The variation of the vortex strength and size and the peak values of the vortex flow quantities ($v_{\theta\,\max}$, $\zeta_{\max}$, and $u_{\mathrm{a,c}}$) with x/c at $\alpha = 10$ deg is summarized in Figs. 5a–5e. Figure 5a reveals that for both the airfoil models tested, the vortex strength grew quite dramatically along the tip of the airfoil and reached a rather constant value at $x/c \approx 1.5$, suggesting that the roll up of the tip vortex, other than the outer region, was nearly complete a half-chord downstream of the trailing edge. The vortex strength was determined by employing Stokes' theorem to compute the circulation about each grid point. For $1.3 < x/c < 3$, the normalized values of total circulation $\Gamma_0/u_\infty c$, were 0.36 and 0.26 for the cambered and symmetric airfoils, respectively. The core vortex strength Γ_c had a constant fraction ($\approx 74\%$) of Γ_0, which is consistent with the theoretical value of $\Gamma_c/\Gamma_0 = 0.715$ of Lamb's[11] solution. Figure 5b indicates that the vortex diameter increased slightly with x/c and was accompanied by a minor decrease or decay in $v_{\theta\,\max}$ and $\zeta_{\max}$ (Figs. 5c and 5d) and that for $x/c \geq 1.15$ both airfoils had similar and somewhat constant core radii ($r_c \approx 0.062c$). The cambered airfoil, however, was found to have larger $v_{\theta\,\max}$ and $\zeta_{\max}$ values but a smaller r_o, and also a higher average $u_{\mathrm{a,c}} = 1.2u_\infty$ for $1.5 < x/c < 2.5$ compared to a $u_{\mathrm{a,c}}$ of $1.07u_\infty$ of the NACA 0015 airfoil (Fig. 5e).

The influence of α on the tip-vortex flow characteristics at $x/c = 1.5$ is presented in Fig. 6. For both of the airfoils, the increase in lift force or α resulted in a basically linear increase in the vortex strength, $v_{\theta\,\max}$, $\zeta_{\max}$, and $u_{\mathrm{a,c}}$ attributed to the increase in the

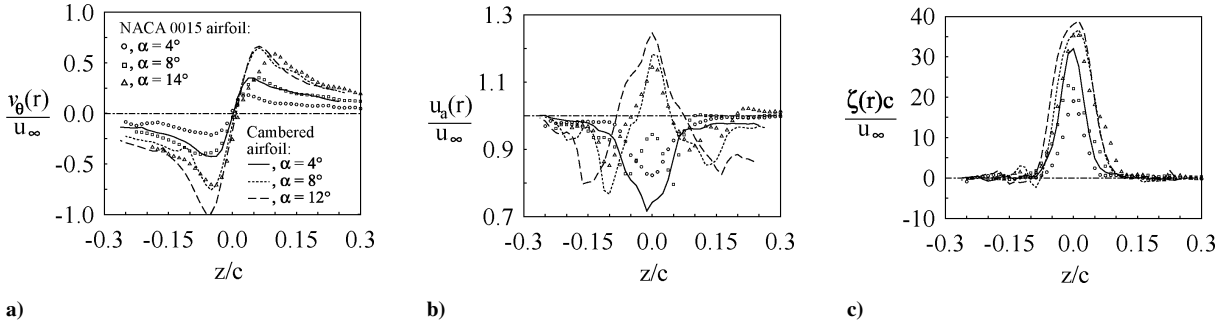

Fig. 4 Typical flow structures across the vortex center.

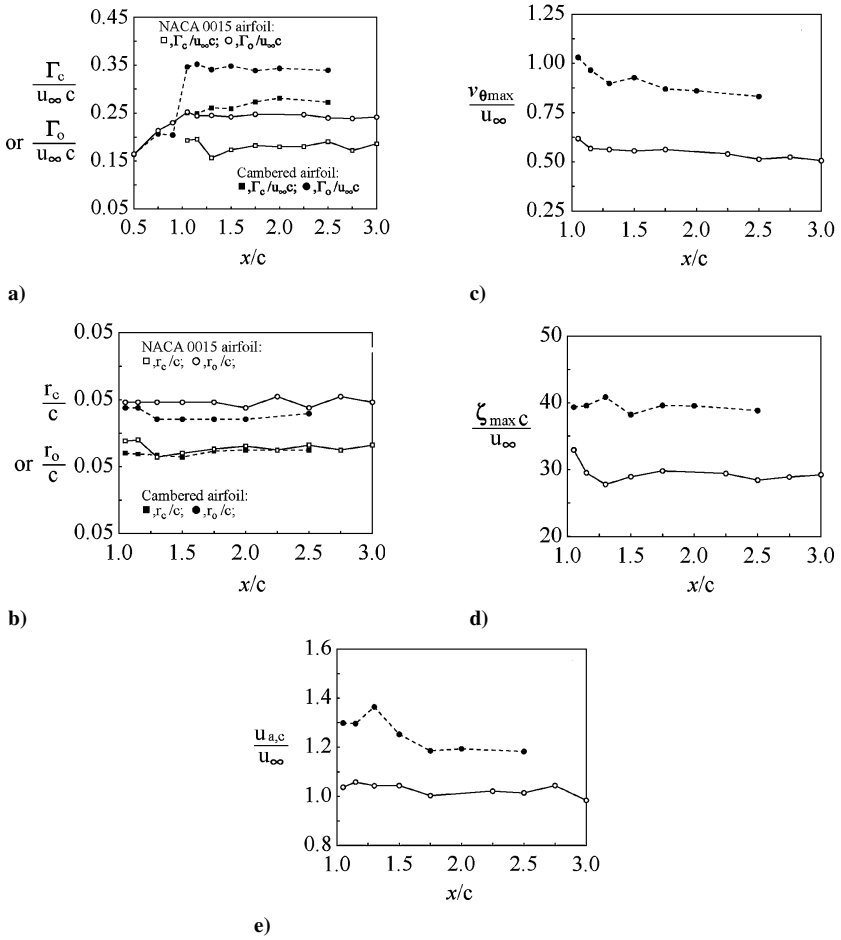

Fig. 5 Vortex structure and strength as functions of *x/c* at $\alpha = 10$ deg.

vorticity shed into the vortex sheet from the boundary layer during its rolling up into a tip vortex along the tip of the wing model. The vortex radius, however, did not appear to have a clear dependence on the circulation and continued to increase for $\alpha > \alpha_{ss}$. The variation of $v_{\theta\,\max}$, $\zeta_{\max}$, and $u_{a,c}$ followed trends similar to the circulation. The cambered airfoil, however, had higher jet-like core flow but a lower wake-like value.

C. Universal Behavior of the Inner Tip-Vortex Flow

The radial distribution of the circulation $\Gamma(r)$ of the tip vortex, normalized by the circulation of the vortex core Γ_c and plotted against $\log(r/r_c)$ for $1.3 < x/c < 3$ and $\alpha = 10$ deg, is presented in Fig. 7a. For $x/c > 1.3$, the distribution of circulation within the tip-vortex core followed a $\Gamma \propto r^2$ profile for $r/r_c < 0.4$ and varied logarithmically for $0.5 < r/r_c < 1.4$. For $r/r_c > 1.4$, Γ continued to vary with x/c, attributing to the fact that at $r > 1.4r_c$ the roll up of the vortex was only nearly complete, and, therefore, there was a slow addition of vorticity to the outer layers of the vortex from the shear layer arriving from the inboard regions.[19] The observed universal behavior of the inner region of a nearly axisymmetric tip vortex in the near-wake region is of particular interest because it generally takes a distance of several tens or even hundreds of wing chords downstream for the vortex to become fully developed and attain the characteristics of asymptotic trailing vortices. The empirical curve-fit relationships that describe the inner-core region and the region where the $\Gamma(r)$ distribution is logarithmic are

$$\Gamma(r)/\Gamma_c = A(r/r_c)^2 \qquad \text{for} \quad r/r_c < 0.4 \tag{1}$$

$$\Gamma(r)/\Gamma_c = B\log(r/r_c) + C \qquad \text{for} \quad 0.5 < r/r_c < 1.4 \tag{2}$$

The curve-fit constants obtained for both the airfoils tested as functions of x/c and α are listed in Table 1. Moreover, for $1.3 < x/c < 3$, all of the data within $0 < r/r_c < 1.2$ collapsed together onto a sixth-order polynomial (similar to that reported by Ramaprian and

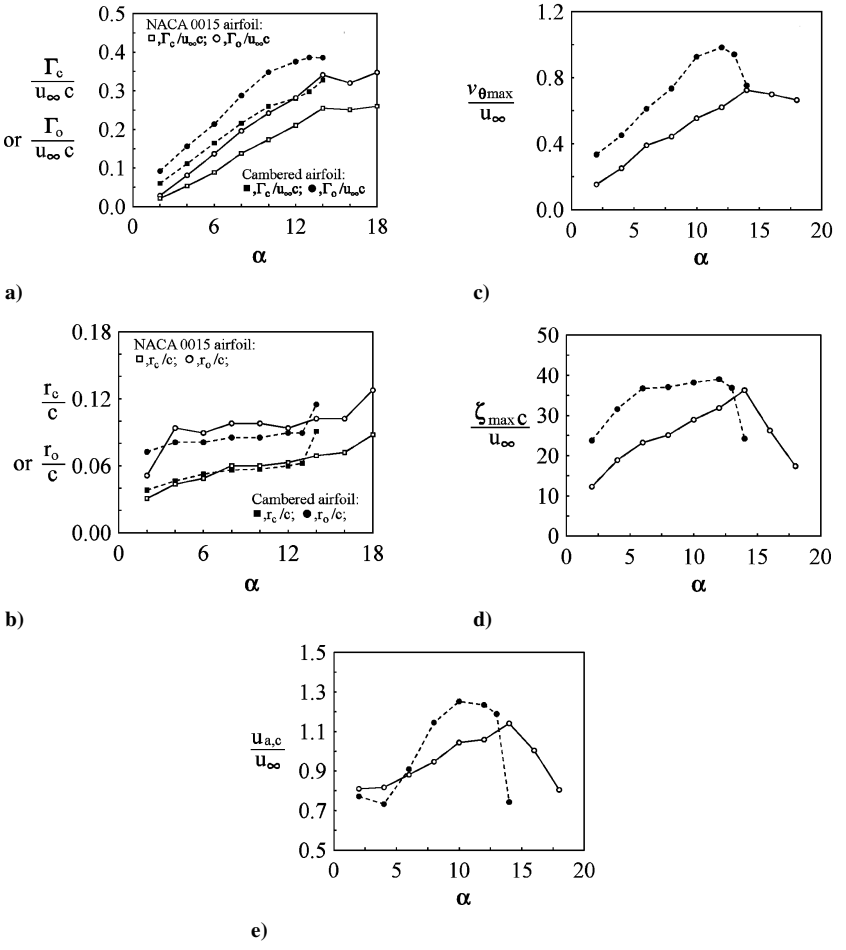

Fig. 6 Vortex structure and strength as functions of α at $x/c = 1.5$.

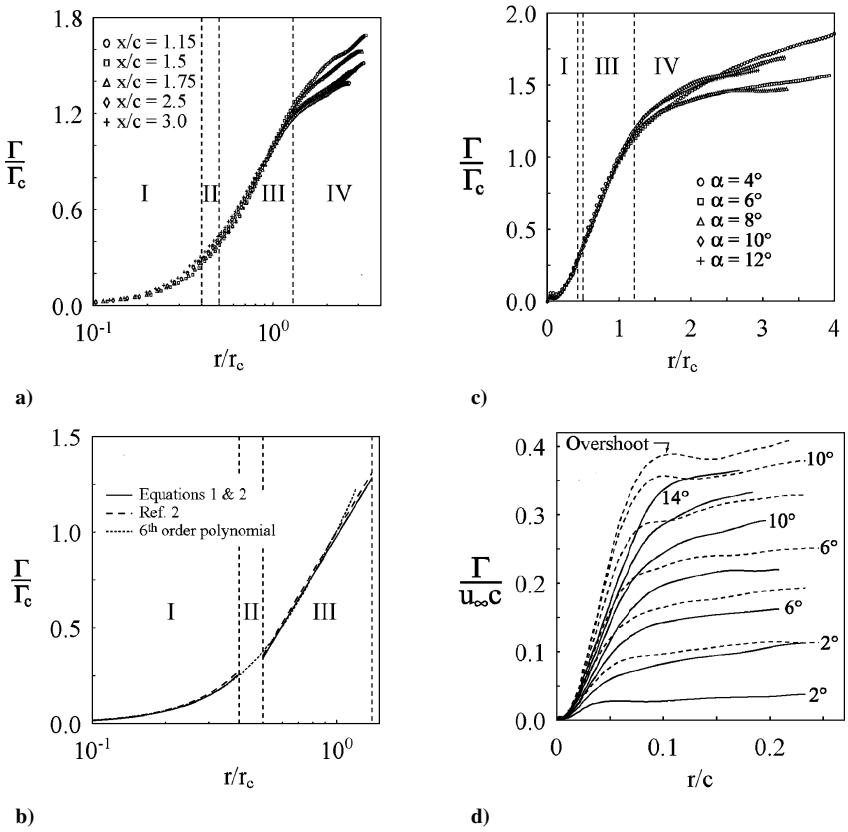

Fig. 7 Radial distribution of circulation: I, inner-core region; II, buffer region; III, logarithmic region; and IV, outer region. For Fig. 7d, ——, NACA 0015 airfoil and . . . ., cambered airfoil.

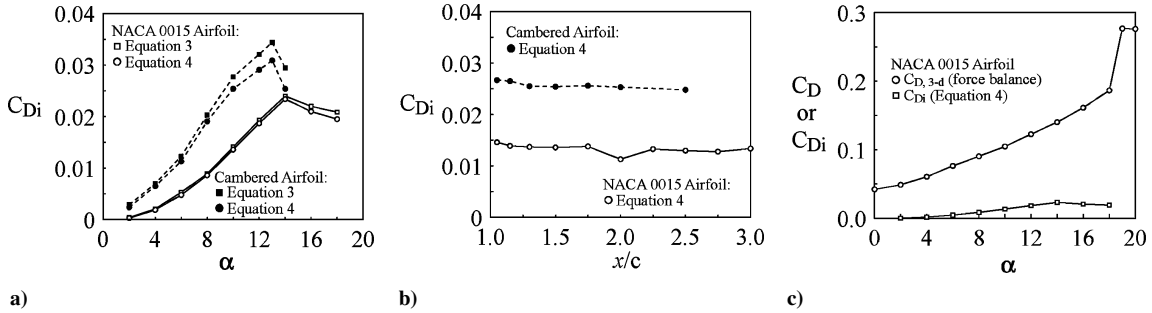

Fig. 8 Variation of induced drag and left-to-drag ratio with α and x/c.

Table 1 Curve-fit constants of Eqs. (1) and (2)

α, deg	A	B	C	x/c	A	B	C
			NACA 0015 airfoil				
4	1.727	1.969	0.994	1.30	1.393	2.215	0.946
6	1.574	1.985	0.955	1.50	1.566	2.230	0.994
8	1.666	2.010	0.972	1.75	1.667	2.110	0.974
10	1.566	2.230	0.994	2.00	1.786	1.942	0.962
12	1.619	1.197	0.978	2.25	1.611	2.208	0.997
14	1.811	2.154	0.986	2.50	1.805	1.927	0.965
16	1.586	2.178	0.994	2.75	1.707	2.042	0.969
18	1.609	2.070	0.970	3.00	2.029	1.893	0.994
			Cambered airfoil				
4	1.681	1.967	0.975	1.30	1.401	2.100	0.977
6	1.462	2.236	1.001	1.50	1.264	2.163	0.937
8	1.526	1.987	0.974	1.75	1.535	1.963	0.956
10	1.264	2.163	0.937	2.00	1.572	2.022	0.962
12	1.377	2.234	0.987	2.50	1.580	1.998	0.961
13	1.416	2.171	0.965	——	——	——	——
14	1.707	2.017	0.965	——	——	——	——

Zheng[18]): $\Gamma(r)/\Gamma_c = 1.756(r/r_c)^2 - 1.044(r/r_c)^4 + 0.263(r/r_c)^6$ for the NACA 0015 airfoil and $\Gamma(r)/\Gamma_c = 1.639(r/r_c)^2 - 0.790(r/r_c)^4 + 0.137(r/r_c)^6$ for the cambered airfoil.

Figure 7b compares the present self-similar, or universal, tip-vortex structures in the near field of a NACA 0015 airfoil with those of Hoffman and Joubert,[2] Phillips,[10] and Ramaprian and Zheng.[18] It is clear that the present measurements are in good agreement with the published results. The universal $\Gamma(r)/\Gamma_c$ behavior was also observed for $\alpha = 4 - 16$ deg at $x/c = 1.5$ (Fig. 7c). A direct comparison of the levels and radial growth of the vortex strength $\Gamma(r)/u_\infty c$, plotted against the radius r/c of the tip vortex at different α for both the airfoils tested, is also summarized in Fig. 7d. Figure 7d shows that other than the significantly increased level of circulation, overshoots of the circulation were also observed for $\alpha = 8 - 14$ deg of the cambered airfoil.

D. Induced Drag

For low-Mach-number and adiabatic flows, the induced drag D_i acting on a wing model with a three-dimensional configuration, can be obtained from[12,13]

$$D_i = \iint_{S2} \frac{1}{2}\rho_\infty (v^2 + w^2)\,\mathrm{d}y\,\mathrm{d}z \tag{3}$$

The induced drag can also be computed from the vorticity using the Maskell induced-drag model.[21] For the Maskell model the crossflow velocity vectors within the measurement plane are decomposed into a stream function $\psi(y, z)$ and a velocity potential $\phi(y, z)$ with the imposed boundary conditions requiring both ψ and ϕ to be zero on the edges of the measurement surface. The induced drag can then be obtained by

$$D_i = \frac{1}{2}\rho_\infty \iint_{S\zeta} \psi\zeta\,\mathrm{d}y\,\mathrm{d}z - \frac{1}{2}\rho_\infty \iint_{S1} \phi\sigma\,\mathrm{d}y\,\mathrm{d}z \tag{4}$$

where the surface S_ζ is the region within $S1$ where the vorticity is nonzero and the flow is incompressible.

Figure 8a shows a comparison of the induced drag coefficients calculated by Eqs. (3) and (4) for a tip vortex at $x/c = 1.5$. It can be clearly seen that for a nearly axisymmetric tip vortex with small streamwise gradients, the two results agree well with each other. Figures 8a and 8b show that the values of C_{Di} [from Eq. (4)] increased with $\alpha(<\alpha_{ss})$ but varied slightly with x/c in the near-wake region. As expected, the cambered airfoil with higher lift was found to generate much higher induced drag. For a NACA 0015 airfoil, the induced drag was found to contribute to no more than 20% of the total drag of a three-dimensional configuration wing model, determined directly with a force balance at $Re = 2.01 \times 10^5$ (Fig. 8c).

IV. Conclusions

The three-dimensional flow structure of a tip vortex generated in the near wake behind both a rectangular, squared-tipped NACA 0015 airfoil and a high-lift cambered airfoil was investigated at $Re = 2.01 \times 10^5$. For both airfoils tested, the tip region was dominated by the strong interaction between the multiple secondary vortices and the main vortex. The roll up was almost complete at $x/c \approx 1.5$, and the overall circulation of the tip vortex remained nearly constant up to $x/c = 3$ (two chord lengths downstream of the trailing edge). As the airfoil incidence increased, the increase in the lift force resulted in a basically linear increase in the vortex strength and the peak values of the tangential velocity and vorticity. The vortex radius, however, did not appear to have a clear dependence on the vortex strength. Depending on the angle of attack, the axial velocity in the core could be either greater than or less than u_∞, that is, either jet-like or wake-like. The normalized circulation within the inner region of the nearly axisymmetric tip vortex exhibited a universal, or self-similar structure. For the NACA 0015 airfoil, the induced drag contributed to less than 20% of the total drag and had a smaller tangential velocity but the same core size compared to a cambered airfoil.

Acknowledgment

This work was supported by the Natural Sciences and Engineering Research Council of Canada.

References

[1]*Aviation Week and Space Technology*, 23 June 2003, p. 15.

[2]Hoffmann, E. R., and Joubert, P. N., "Turbulent Line Vortices," *Journal of Fluid Mechanics*, Vol. 16, 1963, pp. 395–411.

[3]Batchelor, G. K., "Axial Flow in Trailing Line Vortices," *Journal of Fluid Mechanics*, Vol. 20, 1964, pp. 645–658.

[4]Williams, G. M., "Viscous Modeling of Wing-Generated Trailing Vortices," *Aeronautical Quarterly*, Vol. 25, 1974, pp. 143–154.

[5]Donaldson, C. duP., Snedeker, R. S., and Sullivan, R. D., "Calculation of Aircraft Wake Velocity Profiles and Comparison with Experimental Measurements," *Journal of Aircraft*, Vol. 11, No. 9, 1974, pp. 547–555.

[6]Green, S. I., and Acosta, A. J., "Unsteady Flow in Trailing Vortices," *Journal of Fluid Mechanics*, Vol. 227, 1991, pp. 107–134.

[7]Ragab, S., and Sreedhar, M., "Numerical Simulation of Vortices with Axial Velocity Deficits," *Physics of Fluids*, Vol. 7, No. 3, 1995, pp. 549–558.

[8]Zeman, O., "The Persistence of Trailing Vortices: A Modeling Study," *Physics of Fluids*, Vol. 7, No. 1, 1995, pp. 135–143.
[9]Spalart, P. R., "Airplane Trailing Vortices," *Annual Review of Fluid Mechanics*, Vol. 30, 1998, pp. 107–138.
[10]Phillips, W. R. C., "The Turbulent Trailing Vortex During Roll-Up," *Journal of Fluid Mechanics*, Vol. 105, 1981, pp. 451–467.
[11]Lamb, H., *Hydrodynamics*, 6th ed., Dover, New York, 1945, p. 592.
[12]Brune, G. W., "Quantitative Low-Speed Wake Surveys," *Journal of Aircraft*, Vol. 31, No. 2, 1994, pp. 249–255.
[13]Kusunose, K., "Development of a Universal Wake Survey Data Analysis Code," AIAA Paper 97-2294, 1997.
[14]Francis, T. B., and Katz, J., "Observations on the Development of a Tip Vortex on a Rectangular Hydrofoil," *Journal of Fluids Engineering*, Vol. 110, 1988, pp. 208–215.
[15]Shekarriz, A., Fu, T. C., Katz, J., and Huang, T. T., "Near-Field Behavior of a Tip Vortex," *AIAA Journal*, Vol. 31, No. 1, 1993, pp. 112–118.
[16]Devenport, W. J., Rife, M. C., Liapis, S. I., and Follin, G. J., "The Structure and Development of a Wing-Tip Vortex," *Journal of Fluid Mechanics*, Vol. 312, 1996, pp. 67–106.
[17]Chow, J. S., Zilliac, G. G., and Bradshaw, P., "Mean and Turbulence Measurements in the Near Field of a Wingtip Vortex," *AIAA Journal*, Vol. 35, No. 10, 1997, pp. 1561–1567.
[18]Ramaprian, B. R., and Zheng, Y., "Measurements in Rollup Region of the Tip Vortex from a Rectangular Wing," *AIAA Journal*, Vol. 35, No. 12, 1997, pp. 1837–1843.
[19]McAlister, K. W., and Takahashi, R. K., "NACA 0015 Wing Pressure and Trailing Vortex Measurements," NASA TP-3151, 1991.
[20]Wenger, C. W., and Devenport, W. J., "Seven-Hole Pressure Probe Calibration Utilizing Look-Up Error Tables," *AIAA Journal*, Vol. 37, No. 6, 1999, pp. 675–679.
[21]Maskell, E., "Progress Towards a Method for the Measurement of the Components of the Drag of a Wing of Finite Span," Royal Aircraft Establishment, TR 72232, 1973.